Structural and magnetic aspects of $La_4(Co_{1-x}Ni_x)_3O_{10+\delta}$ ($0 \leq x \leq 1$)

Marius Uv Nagell[a], Susmit Kumar[a], Magnus H. Sørby[b], Helmer Fjellvåg[a*] and Anja Olafsen Sjåstad[a]

[a]*Centre for Materials Science and Nanotechnology, Department of Chemistry, University of Oslo, POBox 1033, N-0315 Oslo, Norway*

[b]*Institute for Energy Technology, N-2027 Kjeller, Norway*

*Corresponding author: helmer.fjellvag@kjemi.uio.no

Structural and magnetic aspects of $La_4(Co_{1-x}Ni_x)_3O_{10+\delta}$ ($0 \leq x \leq 1$)

The Ruddlesden-Popper (RP3) type oxides, $La_4Co_3O_{10+\delta}$ and $La_4Ni_3O_{10+\delta}$, form a complete solid solution. Powder X-ray and neutron diffraction data show that $La_4(Co_{1-x}Ni_x)_3O_{10+\delta}$ is isostructural to the monoclinic$La_4Co_3O_{10+\delta}$ structure ($P2_1/a$) described for all compositions without any further structural distortions as suggested in literature. A slight elongation of the Co/Ni-O bonds facing the rock salt interlayer occurs for Ni-rich compositions. The magnetic properties of the solid solution series are mapped in the temperature range from 4 K to 300 K, and the results are presented in a magnetic phase diagram. Three regimes with antiferromagnetic order (AF) exist at low temperatures, $T_N < 10 - 30$ K. For $x = 0.00$ the AF is ascribed to Co(II), whereas a broader AF regime around $x = 0.50$ is ascribed mainly to Ni(II). Pauli paramagnetism is observed close to metallic $La_4Ni_3O_{10+\delta}$, $x > 0.80$. The possibility to tune the oxidation state of the transition metal atoms is demonstrated for $La_4Co_3O_{10+\delta}$, and exemplified by weakening of a temperature induced spin transition at around 480 K.

Crystal structure; Ruddlesden-Popper; magnetization; magnetic susceptibility; differential scanning calorimetry, neutron diffraction

1. Introduction

The solid solution between the two Ruddlesden-Popper (RPn; n = 3) type oxides, $La_4Co_3O_{10+\delta}$ and $La_4Ni_3O_{10+\delta}$ is candidate for electrodes in solid-oxide fuel cells.[1,2] Furthermore, the solid solution has fundamental interest since it combines structurally similar compounds with major differences in electronic properties. The Co-phase is paramagnetic at room-temperature and antiferromagnetic below 12 K,[3] whereas $La_4Ni_3O_{10+\delta}$ shows temperature independent Pauli paramagnetism and good electrical conductivity.[4] Interestingly, for the corresponding Nd-RP3 nickelate, an electronic metal-to-metal transition occurs at around 165 K.[4] The metallic like behaviour of the nickel based compound concurs with the metallic nature of $LaNiO_3$ with formally trivalent nickel.[5] These complex oxides take the basic RP3-type atomic arrangement, with a slight monoclinic distortion for $La_4Co_3O_{10+\delta}$ according to synchrotron and neutron powder diffraction data.[3,6] Such a distortion has indeed also been found for the corresponding Nd-based cobaltite and nickelate RP3s.[7] The structure of $La_4Ni_3O_{10+\delta}$ was first described in space group *Fmmm* by Zhang and Greenblatt.[4] Symmetry lowering to *Imm2* was indicated by electron diffraction, whereas Tkalich *et al.* obtained best fit to their powder neutron diffraction (PND) data for space group *Cmca*.[8] Interestingly, Amow *et al.* suggests a series of different structural distortions as function of composition x for the solid solution, $La_4(Co_{1-x}Ni_x)_3O_{10+\delta}$ with possible space groups *Bmab* for ($0.00 \leq x \leq 0.13$, $0.33 \leq x \leq 0.73$, and $0.93 \leq x \leq 1.00$) and *Fmmm* for ($0.20 \leq x \leq 0.27$, and $0.80 \leq x \leq 0.87$).[1] These findings were based on X-ray diffraction data from the home laboratory. In this work we revisit the crystal structure of the solid solution by means of powder neutron diffraction (PND). The scattering contrast provided by neutrons for oxygen atoms relative to the heavy cations

can help settling open issues since structural distortions are likely rooted in tilting of the $(Co,Ni)O_6$-octahedra within the triple perovskite blocks of the RP3 structure.

The average oxidation state for the *3d* cation in the $(Co,Ni)O_6$-octahedra is +2.67.The low antiferromagnetic ordering temperature for $La_4Co_3O_{10+\delta}$ is consistent with a simple ionic picture of two Co(III) low-spin (S = 0) cations and one Co(II) high-spin cation per formula unit. Notably, the average oxidation state of cobalt is tuneable, since additional oxygen atoms can be intercalated into the rock salt (RS) layers that separate the perovskite blocks. The hitherto maximum value of δ = 0.30 corresponds to an average Co-oxidation state of + 2.87.[3] For $La_4Ni_3O_{10+\delta}$ the average oxidation state of +2.67 is approaching that formally found in metallic $LaNiO_3$. For $La_4Ni_3O_{10+\delta}$ there are reports on partly reduced and oxidized variants with δ = –0.22 and 0.12,[9] however it is fair to claim it remains open whether higher oxygen content variants ($\delta > 0.00$) exist.

The current paper reports on synthesis, physical characterization and crystal structure of the $La_4(Co_{1-x}Ni_x)_3O_{10+\delta}$ solid solution. Furthermore, the possibility to tune the oxygen content, δ, by annealing at selected pO_2 atmosphere – temperature conditions is exemplified for x = 0.00 and 1.00. The crystal structure is reported for x = 0.00, 0.20, 0.47, 0.80, 0.93, and 1.00 based on Rietveld refinement of powder neutron diffraction data at ambient temperature. The magnetic and electronic properties in the temperature interval from 4 K to 300 K are described on the basis of PPMS measurements and neutron diffraction data, and a magnetic phase diagram is provided for $T < 50$ K.

2. Experimental

Samples of $La_4(Co_{1-x}Ni_x)_3O_{10+\delta}$ ($0 \leq x \leq 1$) were synthesized according to the citric acid method following standard procedures for our laboratory.[3,6,7] The starting materials were La_2O_3 (99.99 %, Molycorp), $Ni(CH_3COO)_2 \cdot 4H_2O$ (≥ 99.0 %, Sigma

Aldrich), $Co(CH_3COO)_2 \cdot 4H_2O$ (reagent grade, Sigma Aldrich), and citric acid monohydrate, $C_3H_4(OH)(COOH)_3 \cdot H_2O$ (98 %, Sigma Aldrich). In order to remove water and carbon dioxide, La_2O_3 was calcined at 800 °C and cooled in a desiccator before use. From gravimetric analysis exact formula weights of the cobalt and nickel acetate salts were determined. La_2O_3 was first dissolved in a mixture of HNO_3 (68 %, VWR Chemicals) and de-ionised water (volume ratio 1 : 1). The cobalt and nickel acetates, dissolved in de-ionised water, were then added. Citric acid monohydrate was added during stirring and heating of the entire solution. The solution was left boiling until all nitrates was decomposed as nitrous gases, and then dehydrated in a heating cabinet at 180 °C overnight. Thereafter, calcination was done at 450 °C for 24 h in static air. Cold-pressed pellets of the obtained grey to black powders were annealed in tube furnaces at 1000 – 1100 °C, in either flowing nitrogen (5N, Aga) ($0.00 \leq x \leq 0.33$) or static air ($0.33 < x \leq 1.00$), two or more times, with intermediate grinding and re-pelletizing between each annealing. The holding times varied between 24 and 48 h. Phase purity was ascertained by powder X-ray diffraction (XRD), and oxygen content was determined by cerimetric titrations and thermogravimetric analysis (TGA). Magnetic studies on $La_4Co_3O_{10+\delta}$ were conducted for finely crushed powders (denoted 0.00S), for coarse particles 0.00L), and for sintered specimen.

Cerimetric titrations were performed by dissolving Mohr salt, $(NH_4)_2Fe(SO_4)_2 \cdot 6H_2O$ (99 %, Sigma-Aldrich), and a small amount of the sample in 1 M HCl in inert atmosphere of Ar (5N, Aga). The solution was thereafter titrated with 0.1 M $Ce(SO_4)_2$ (volumetric, Fluka) under inert atmosphere of flowing Ar. Exact formula weight of the Mohr salt was determined gravimetrically (4 parallels). The exact concentration of the $Ce(SO_4)_2$ solution was determined separately by titrating with Mohr salt.

Thermogravimentric (TGA) and differential scanning calorimetric (DSC) analysis in N_2 (5N Aga), O_2 (5N Aga), and O_2/N_2-atmospheres were performed with a Netzsch STA 449 F1 Jupiter. Heating and cooling were performed at rates of 10 °C/min. Background corrections were measured with empty sample holders at identical experimental conditions to eliminate any effects from the holders and the atmosphere.

Room temperature powder X-ray diffraction (XRD) data were collected with a Bruker D8 Discover with a Lynxeye detector and using Cu$K\alpha_1$ radiation from a Ge(111) Johansson monochromator. Diffraction data were collected at room temperature between 2θ = 10° and 90°. Unit cell dimensions were determined by profile refinements using Pawley fitting [10] with the program TOPAS.[11]

Powder neutron diffraction (PND) data are collected using the two-axis PUS powder diffractometer at the JEEP II reactor at IFE, Kjeller, Norway. The wavelength of the monochromatized neutrons was 1.5545 Å. Data were collected at room temperature between 2θ = 10° and 130° and at 8 K between 2θ = 4° and 130° in steps of $\Delta(2\theta)$ = 0.05°. Rietveld analysis of the PND data was performed with the GSAS program package.[12] 2398 data points, 1360 Bragg reflections, and a maximum of 61 variables entered into the least squares refinements. The background was modelled by a cosine Fourier series polynomial, and the peak shapes described by a pseudo-Voigt function. Distance restraints were introduced for the CoO_6 and NiO_6 octahedrons, as well as for the La–O-distances. The Co/Ni-O distances were restrained to 1.95 Å (± 0.04 Å), the La-O distances to 2.65 Å (± 0.45 Å), and using a penalty factor of 100. U_{iso} for the Co/Ni atoms were constrained to half of U_{iso} for the La-atoms. The obtained R-factors were typically $R_{wp} \approx 8$ with $R_{exp} \approx 5$.

Magnetic property data were measured using a Quantum Design Physical Property Measurement System (PPMS) in the temperature range from 4 to 300 K. All samples

were held in gelatine capsules and studied at both zero field cooled (ZFC) and field cooled (FC) conditions, and measured upon heating. An applied magnetic field of 500 G was used. Measurements of magnetization at 4 K – 70 K were performed for various applied fields up to 9 Tesla.

3. Results and discussion

3.1. Crystal structure.

Phase pure samples of the complete $La_4(Co_{1-x}Ni_x)_3O_{10+\delta}$ solid solution were obtained by wet chemical synthesis. For all eight investigated samples in the range $0.00 \leq x \leq 1.00$, the (117) Bragg reflection (XRD data) in the orthorhombic description of the RP3 unit cell shows peak broadening, as mentioned by Zhang and Greenblatt.[4] By using the monoclinic unit cell of Fjellvåg *et al.*,[6] the Pawley profile fit is improved and the broadening of (117) is consistent with symmetry lowering to monoclinic. The variation of unit cell dimensions is shown in Figure 1. The *a*- and *b*-axes are fairly constant, whereas the *c*-axis expands with increased Ni-content and the monoclinic distortion diminishes. The unit cell volume is quite constant for $x < 0.50$, where after it increases towards $La_4Ni_3O_{10}$, see Figure 1.

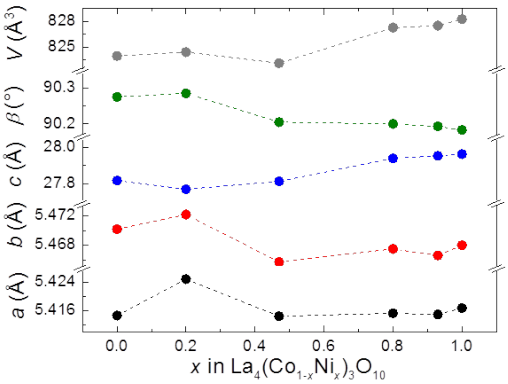

Figure 1. Unit cell dimensions for $La_4(Co_{1-x}Ni_x)_3O_{10}$ at ambient temperature, space group $P2_1/a$.

Crystallographic data obtained from the Rietveld refinements are listed in Table 1, as exemplified by $x = 0.20$. The unit cell dimensions from XRD were used as starting point for the refinements, owing to a better peak resolution. Likewise, the atomic coordinates for $La_4Co_3O_{10+\delta}$, space group $P2_1/a$, were used as starting point. Due to the large number of non-equivalent atoms and the limited resolution and statistics of the PND data, distance restraints were adopted for the La–O and Ni/Co–O separations, see experimental. The refinements gave no indications for any ordering of the Ni and Co atoms, in line with their similar sizes and electronic properties. Representative examples of fitted PND patterns are given in Figure 2. The results for the six examined samples show no major deviations from the presented data in Figure 2 and Table 1.

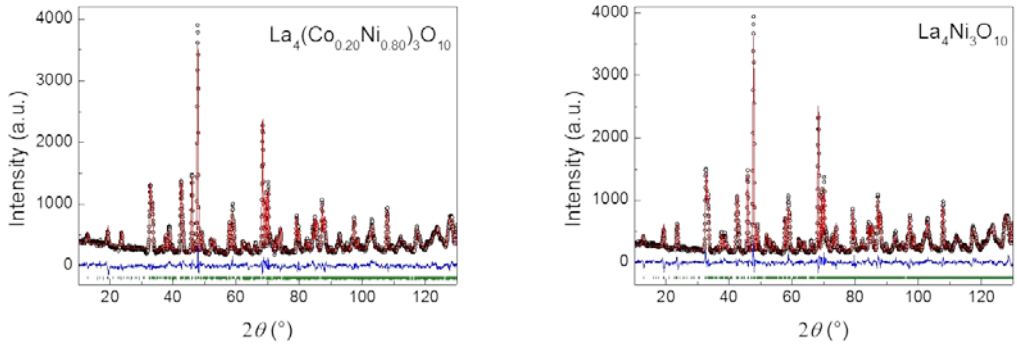

Figure 2. Observed (open circles), calculated (red solid line) and difference (blue solid line) powder neutron diffraction patterns of $La_4(Co_{1-x}Ni_x)_3O_{10}$ at ambient temperature and vertical green bars as positions for reflections, space group $P2_1/a$; left panel $x = 0.80$; right panel $x = 1.00$.

Table 1. Atomic coordinates for $La_4(Co_{1-x}Ni_x)_3O_{10}$ with $x = 0.20$ as derived from Rietveld refinements of PND data at room temperature. Space group $P2_1/a$. Calculated standard deviations in parentheses.

Atom	**Wyckoff position**	***x***	***y***	***Z***	U_{iso} **(10^{-2} Å^2)**
La1	4*e*	0.007(4)	0.000(4)	0.3016(5)	0.32(7)
La2	4*e*	0.496(5)	0.022(3)	0.8038(6)	0.32(7)
La3	4*e*	0.018(4)	1.006(3)	0.4303(6)	0.32(7)
La4	4*e*	0.506(4)	–0.001(3)	0.9311(6)	0.32(7)
(Ni,Co)1	2*b*	0	½	1/2	0.16(4)
(Ni,Co)2	2*a*	0	0	0	0.16(4)
(Ni,Co)3	4*e*	–0.005(7)	–0.003(1)	0.1407(2)	0.16(4)
(Ni,Co)4	4*e*	0.487(6)	0.003(1)	0.6399(2)	0.16(4)
O1	4*e*	0.269(3)	0.269(3)	0.4925(6)	1.11(8)
O2	4*e*	0.284(2)	0.216(2)	0.9979(8)	1.11(8)
O3	4*e*	–0.000(6)	0.032(5)	0.0703(1)	1.11(8)
O4	4*e*	0.490(6)	0.048(4)	0.5698(2)	1.11(8)
O5	4*e*	0.242(5)	0.252(6)	0.1449(6)	1.11(8)
O6	4*e*	0.738(5)	0.250(6)	0.6501(6)	1.11(8)
O7	4*e*	–0.003(7)	0.966(5)	0.2113(3)	1.11(8)
O8	4*e*	0.487(6)	0.977(6)	0.7107(3)	1.11(8)
O9	4*e*	0.753(5)	0.247(6)	0.8701(5)	1.11(8)
O10	4*e*	0.260(5)	0.247(5)	0.3620(6)	1.11(8)

These results prove unequivocally that there are no series of different types of structural distortions throughout the solid solution regime. Hence, $La_4(Co_{1-x}Ni_x)_3O_{10+\delta}$ crystallizes in $P2_1/a$ for all values of *x*, in contrast to the report by Amow *et al.*[1] The RP3 crystal structure is shown in Figure 3, emphasizing the triple perovskite slabs for *x* = 0.00, 0.47 and 1.00. Their crystal structures are close to identical. The sole two

significant variations concern the Co3/Ni3–O7 and Co4/Ni4–O8 bonds, increasing by 0.05 Å on going from the pure cobaltite (x = 0; 1.97 Å) to the pure nickelate RP3 (x = 1; 2.02 Å).

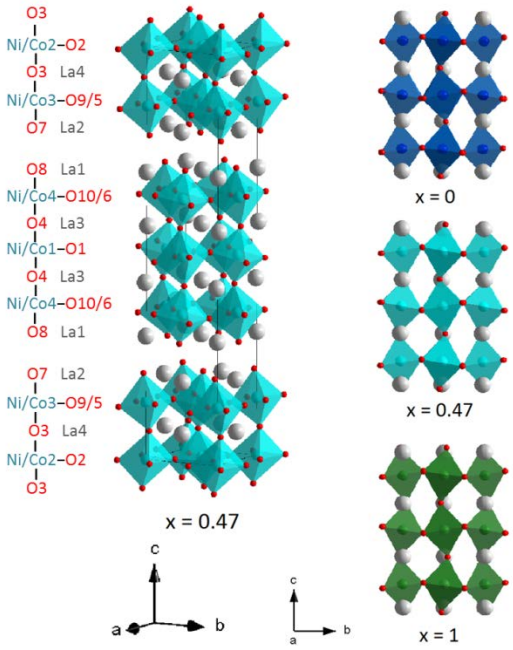

Figure 3. RP3 crystal structure of $La_4(Co_{1-x}Ni_x)_3O_{10}$, x = 0.00, 0.47 and 1.00.

3.2. Oxygen non-stoichiometry.

RP-phases may intercalate anions (oxygen) in tetrahedral interstices of their rock salt type layers. The actual concentration of intercalated atoms is strongly system dependent. For $La_4Co_3O_{10+\delta}$, oxygen rich compositions up to $\delta \approx 0.30$ are reported.[3] For the currently as-synthesized x = 0.00, 0.20, 0.47, 0.80, 0.93, and 1.00 samples (see experimental), cerimetric titration gives an oxygen content very close to the ideal stoichiometry, *i.e.* $\delta = 0.00$ (standard deviations for 3 – 5 parallels are ± 0.02). Within the uncertainty of the method, the oxygen content is therefore considered as 10.00 for all composition x, *i.e.* no oxygen vacancies nor interstitials present.

Excess oxygen in the RS-layer leads to increased formal oxidation states for the Co/Ni-atoms. This may affect magnetic and electric properties. This is currently conveniently illustrated for an anticipated spin-transition in $La_4Co_3O_{10+\delta}$ which is easily observed by DSC.[3] The strong endothermic effect for $La_4Co_3O_{10.00}$ seen at around 200 °C, Figure 4, decreases rapidly upon increased oxygen content δ. For $La_4Co_3O_{10.20}$ no anomaly is any longer observed. The phenomenon has vanished for $La_4(Co_{0.97}Ni_{0.03})_3O_{10.00}$, see insert to Figure 4.

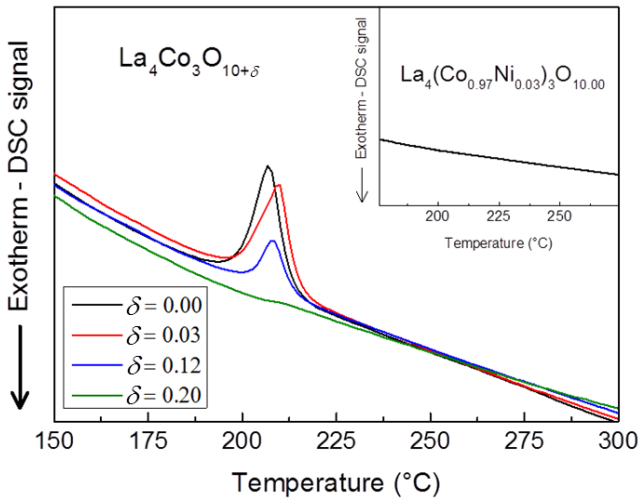

Figure 4. DSC signals for $La_4Co_3O_{10+\delta}$ measured on heating in flowing N_2 for different values of oxygen non-stoichiometry (δ = 0.00, 0.03, 0.12, 0.20). Insert shows corresponding DSC data for $La_4(Co_{0.97}Ni_{0.03})_3O_{10.00}$.

This endothermic anomaly correlates with temperature induced changes in the magnetic susceptibility and with anomalous thermal expansivity. These observations are indicative of a spin transition for the Co(III) cations, from a lower- to a higher- spin state.[3] The current data suggests, however, a more complex explanation. For $La_4Co_3O_{10.00}$ the average Co-oxidation state is +2.67, and strong signatures of the transition are observed, but for $La_4Co_3O_{10.20}$, with average Co-oxidation state +2.80 [formally 2.4 Co(III) and 0.6 Co(II)], the endothermic signal is hardly visible. If the

transition were due to just Co(III), one would rather expect stronger signatures for higher Co(III) contents. In the related $LaCoO_3$ perovskite, a corresponding spin-transition is manifested in terms of anomalies in susceptibility and expansivity,[13, 14, 15] and ascribed to spin changes of Co(III) atoms.

3.3. Magnetic properties at low temperatures

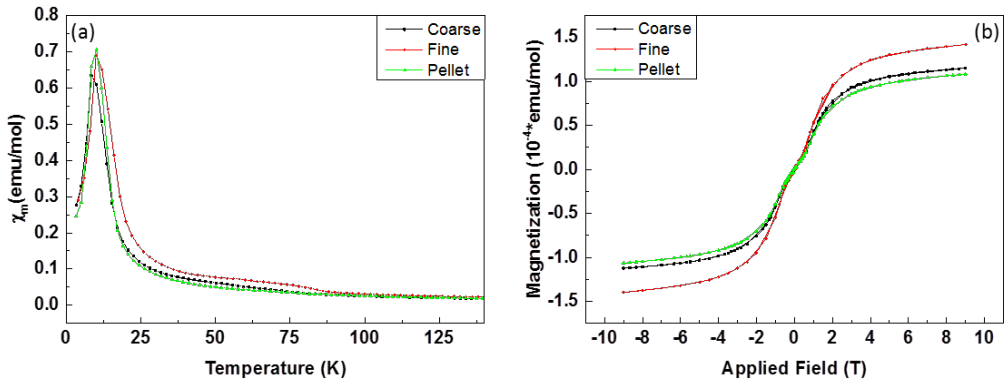

Figure 5. (a) Magnetic susceptibility (χ_m(T)) curves of fine and coarse powder as well as uncrushed, sintered $La_4Co_3O_{10}$. (b) M(H) curve of the same samples at 4 K.

ZFC/FC *M(T)* and *M(H)* data for $La_4(Co_{1-x}Ni_x)_3O_{10}$ reveal complex behaviours. For $La_4Co_3O_{10}$ the magnetic susceptibility at ZFC and FC conditions show Curie − Weiss (CW) paramagnetic behaviour in two temperature ranges; 80 K – 300 K (μ_{eff} = 4.69 μ_B, θ = –3.9 K), and 20 K – 80 K (μ_{eff} = 4.42 μ_B, θ = 1.9 K), similar to observations by Hansteen *et al.*[3] A bifurcation of the ZFC/FC curves is observed at ~ 80 K. This bifurcation shows a weak upward trend for FC conditions relative to ZFC for 10 – 80 K in an applied field of H = 500 G and suggests a weak ferromagnetic state. In some respect $La_4Co_3O_{10}$ thereby mimics $LaCoO_3$ for which Durand *et al.* discussed a weak ferromagnetic effect at low temperature, possibly caused by lattice strain due to traces of a cobalt oxide phase similar to situations encountered for thin-films and

nanoparticles.[16] Recently, Yan *et al.* explained the field dependent properties of $LaCoO_3$ by surface magnetism caused by perturbed Co(III) coordination at the surface of finely crushed oxide particles.[17] Key evidence was provided by Yan *et al.* through comparative studies between small and large particles. The ferromagnetic contribution vanished for large particles, assumingly owing to a low amount of Co(III) surface cations in the bulk samples. A parallel experiment of finely crushed powder and coarse particles (~100 μm) of $La_4Co_3O_{10}$ as well as of large sintered specimens showed a quite similar situation, as shown in Figure 5. Hence, for the fine powders there are additional magnetic features below 80 K that are superimposed on the otherwise paramagnetic or antiferromagnetic bulk properties. On the other hand, the *M(H)* curves at 4 K shows significant hysteresis, along with a large saturation magnetization. The latter field induced transition from an antiferro- to a ferromagnetic state is an intrinsic bulk property of $La_4Co_3O_{10}$, see also below. In this respect $La_4Co_3O_{10}$ differs dramatically from $LaCoO_3$.

Table 2. Weiss Constant (θ), effective paramagnetic moment (μ_{eff}), and calculated spin-only magnetic moment (μ_{calc}) as derived from fit values of the Curie − Weiss law for magnetic susceptibility data of x = 0.00, 0.20, 0.25, 0.33, 0.50, 0.67, and 0.72 in the temperature range 80 K – 300 K.

x	**C (emu K Oe^{-1} mol^{-1}) (±0.02)**	**θ (K)**	**μ_{eff} (μ_B) $(Co_{1-x}Ni_x)_3$**	**μ_{calc} (μ_B) $(Co_{1-x}Ni_x)_3$**
0.72	0.80	–61.7	2.52	2.07
0.67	0.84	–40.3	2.59	3.08
0.50	0.66	4.90	2.29	2.30
0.33	1.19	–38.3	3.08	3.16
0.25	3.01	–5.20	4.91	4.82
0.20	1.68	–31.4	3.66	3.67
0.00L	2.76	–3.90	4.69	4.7–5.2[24]
0.00S	3.42	–1.30	5.23	4.7–5.2[24]

In the case of $LaCoO_3$, experimental and theoretical data suggest a direct transition of trivalent cobalt Co(III) from LS to HS states at T ≈ 90 K.[18,19] It remains controversial whether an intermediate spin state (IS) exist.[20,21,22,23] For $La_4Co_3O_{10}$ the picture is more complicated. The magnetic susceptibility of $La_4(Co_{1-x}Ni_x)_3O_{10}$ follows to a large extent the Curie Weiss Law in the range 80 K − 300 K. The deduced effective paramagnetic moment (μ_{eff}) and the Weiss constant 'θ' are listed in Table 2. For $x > 0.72$ the susceptibility is low and the CW law is not applicable. The derived 'θ' values are consistent with the observed low ordering temperatures, however, an anomalous (positive) value is observed for $x = 0.50$. The effective paramagnetic moment shows a gradual decrease from $x = 0.20, 0.33, 0.67$ to 0.72. According to Table 2 the observed μ_{eff} values are in good agreement with calculated values based on the spin-only approximation when anticipating Co(III) in $3d^6$ low spin (LS), ($t_{2g}^6 e_g^0$)) configuration for all intermediate concentrations except $x = 0.25$. For un-substituted $La_4Co_3O_{10}$, Co(II) is hence the main magnetically contributing ion. The observed effective moment for coarse ($\mu_{eff} = 4.69\ \mu_B$) and fine powders ($\mu_{eff} = 5.26\ \mu_B$) of $La_4Co_3O_{10}$ are within the experimentally reported values for Co(II) with S and L contributions; $\mu_{expt} = 4.7 - 5.2\ \mu_B$.[24] This slight difference in moment is tentatively explained by increase in the surface to volume ratio, and hence additional contributions from Co(III) with perturbed local structure at the surface. For $x = 0.72$ ($\mu_{eff} = 2.26\ \mu_B$; $\mu_{calc} = 2.59\ \mu_B$; respectively) Co(II) will be fully replaced with Ni(II) [$3d^8$ HS ($t_{2g}^6 e_g^2$)], whereas Ni(III) [$3d^7$ LS ($t_{2g}^5 e_g^2$)] will replace some Co(III)-LS ions; see below for further discussion of electronic states of Co- and Ni-ions in the solid solution phase.

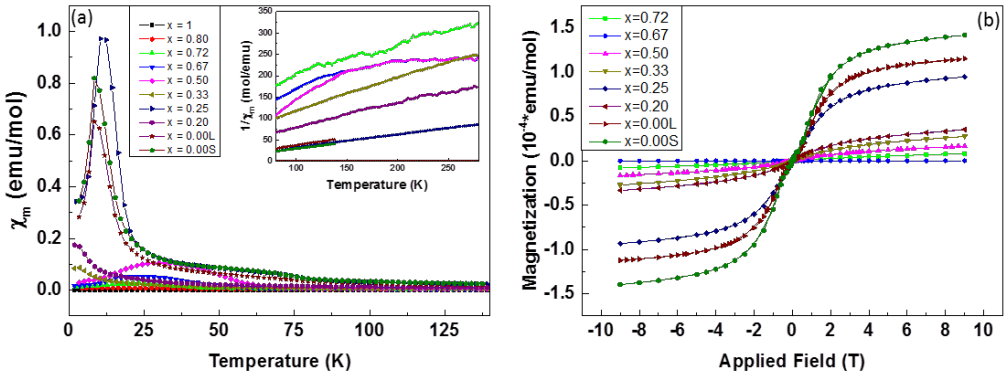

Figure 6. Left; temperature dependence of the magnetic susceptibility $\chi_m(T)$ for $La_4(Co_{1-x}Ni_x)_3O_{10}$ $0.00 \leq x \leq 1.00$; x compositions are x = 0.00S, 0.00L, 0.20, 0.25, 0.33, 0.50, 0.67, 0.72, 0.80, and 1.00; insert shows $\chi^{-1}(T)$. Right; *M(H)* data for fields up to 9 T at a temperature of 4 K for all concentrations except x = 0.80 to 1.00.

The second CW region at low temperature (10 K – 80 K) for $La_4Co_3O_{10}$ has a lower effective magnetic moment of μ_{eff} = 4.4 μ_B, still within the range expected for Co(II). Upon further cooling, the ZFC and FC curves gradually peak at $T_N \approx 13$ K marking onset of antiferromagnetic order (AF-1), Figure 6, in accordance with Hansteen *et al.*[3,25] and supported by current AC magnetization data. Importantly, the *M(H)* data in Figure 6 show a field induced transition from the AF-1 to a ferromagnetic FM state and saturation in high fields. The ordered magnetic moment per formula unit is estimated as 2.7 μ_B based on the saturation magnetization at 4 K. Anticipating that the moment is entirely attributed to Co(II), this implies a moment of 2.7 μ_B per Co(II) atom. Interestingly, similar yet weaker features are observed for x = 0.25, see Figure 6, where saturation magnetizations gives 2.3 μ_B per formula unit.

The current study on $La_4Ni_3O_{10}$ complies with weak Pauli paramagnetism and metallic behaviour below 300 K.[7] Weak additional features such as an inflection point at 160 K and a resistivity minimum at 140 K are reported.[8,26] After noise reduction, we

observe as very faint features a ZFC minimum at 90 K and a drop in susceptibility at 112 K. The conductivity is explained in terms of oxygen $2p_\sigma$ and the nickel *3d* states ($2p_\sigma$-e_g bonding and antibonding).[27] It has been proposed that the triple perovskite slabs in $La_4Ni_3O_{10}$ may be described in terms of Ni(III) layers sandwiching a central Ni(II) layer. The current PND data provides no support for any such Ni-charge ordering, and our bond valence calculations show no significant differences between the four non-equivalent Co/Ni-atoms.

The samples $0.20 < x \leq 1.00$ do not follow the Curie-Weiss law in the 10 K – 80 K temperature range. On introducing nickel into $La_4Co_3O_{10}$ the AF-1 order vanishes and $x = 0.20$ shows Curie-Weiss paramagnetism in the range 2 K – 300 K. For $x = 0.25$, a clear antiferromagnetic transition is observed at $T_N = 10$ K in the ZFC data (AF-2). AC magnetization data show no frequency dependency at $T_N = 10$ K, which otherwise could be indicative of spin-glass like situations. At $x = 0.42$, the ZFC curve shows a prominent antiferromagnetic transition at $T_N = 20$ K (AF-3), Figure 7. Again AC-magnetization shows no frequency dependence. For $x = 0.47$, the AF-3 transition temperature is increased to $T_N = 30$ K. For $x = 0.58$, the ZFC curve shows onset of AF-3 order at $T_N = 28$ K.

Powder neutron diffraction data were collected at 8 K (see above for crystallographic data). However, they did not reveal any magnetic reflections at 8 K for the AF-states of the intermediate *x*-compositions. Hence, their ordered magnetic moments are anticipated to be less than 0.5 μ_B/per average (Co, Ni)-atom. We add that also for $La_4Co_3O_{10}$ the AF-reflections are quite weak in the neutron diffractions patterns, and no details are at hand on the AF-1 spin orientations.[25]

3.4. Phase diagram

The low temperature magnetic phase diagram for $La_4(Co_{1-x}Ni_x)_3O_{10}$ is sketched in Figure 7. The existence of two intermediate antiferromagnetic phases for $0.20 \leq x \leq 0.80$ is notable. It is likely that the three antiferromagnetic regimes denoted AF-1, AF-2 and AF-3 represent different magnetic structures. Of these, only AF-1 has been proved by neutron diffraction.[25]

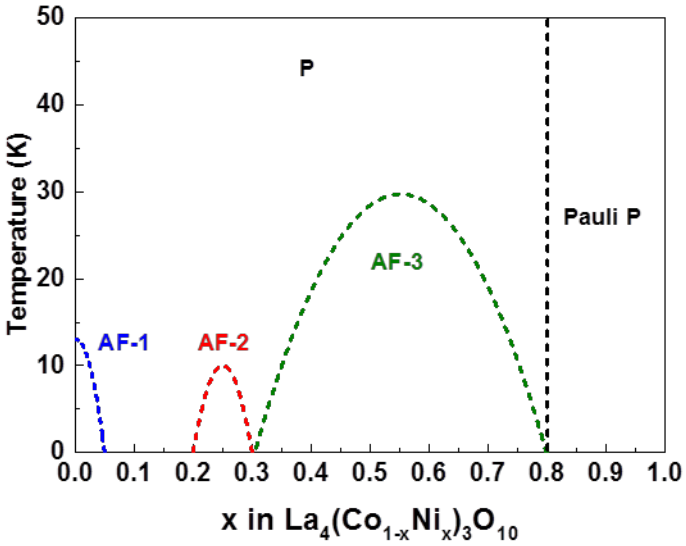

Figure 7. Low-temperature magnetic phase diagram for $La_4(Co_{1-x}Ni_x)_3O_{10}$.

In the $La_4(Co_{1-x}Ni_x)_3O_{10}$ solid solution, Co- and Ni-atoms are randomly distributed on octahedral sites according to PND data. There are no evidences for charge ordering. The AF-1 state for $x = 0.00$ is due to Co(II) atoms in the triple perovskite type blocks, with Co(III) being mainly non-magnetic $3d^6$ low-spin. The AF-3 regime centred on $x \approx 0.50$ has a different origin. Since Ni(III) is less stable than Co(III) at a given T, pO_2 condition, a substitution of cobalt into $La_4Ni_3O_{10}$ would imply that Ni(III) atoms are exchanged by Co(III) atoms, which enhances the Ni(II) concentration. A possible description of $La_4(Co_{0.50}Ni_{0.50})_3O_{10}$ is $La_4Co(III)_{1.5}Co(II)_0Ni(III)_{0.5}Ni(II)_1O_{10}$. Anticipating that Co(III) is LS, and Ni(III) is not the main source for unpaired electrons,

it is likely that AF-3 is mainly due to Ni(II). In octahedral fields, Ni(II) has two unpaired electrons, which, when averaged for the *3d*-sublattice gives an ordered magnetic moment that easily escapes detection by neutron diffraction. Along the same line of arguments, introduction of nickel into $La_4Co_3O_{10}$ will likely imply exchange of Co(II) by Ni(II), thereby weakening the magnetic interactions and loss of cooperative magnetism, see Figures 6 and 7. According to Shannon, ionic radii for coordination number six are Co(II) HS 0.745 Å, Co(III) HS 0.61 Å, Co(III) LS 0.545 Å, Ni(II) 0.690 Å and Ni(III) LS 0.56 Å.[28] Hence, at substitution levels $x > 0.50$, the small sized Co(III) LS atoms will be replaced by somewhat larger Ni(III) atoms, consistent with the $V(x)$ volume expansion shown in Figure 1 for $x > 0.50$. The border between Curie-Weiss paramagnetism and Pauli paramagnetism is indicated at $x = 0.80$ in Figure 7. A remaining open question is how the electric conductivity varies across this border.

4. Conclusion

The crystal structure of the $La_4(Co_{1-x}Ni_x)_3O_{10}$ solid solution phase retains monoclinic $P2_1/a$ symmetry for all compositions of *x*, thereby settling issues in literature with multiple phase changes as function of *x*-composition. The magnetic phase diagram bridges semiconducting, antiferromagnetic $La_4Co_3O_{10}$ and metallic, Pauli paramagnetic $La_4Ni_3O_{10}$ and exhibits a richness of novel magnetic features at intermediate compositions. $La_4Co_3O_{10}$ transforms into a ferromagnetic state at high magnetic fields, and anomalies in susceptibility as well as hysteresis in *M(H)* are proven to be of different origin than in $LaCoO_3$, where striking features are related to surface magnetism of perturbed Co(III) octahedral sites. For finely ground powders, additional ferromagnetic like features are observed for $La_4Co_3O_{10}$ below 80 K, possibly having the same origin as recently postulated for a perturbed surface structure of Co(III) in $LaCoO_3$.

5. Acknowledgements

Henrik Sønsteby is gratefully acknowledged for assistance with operation of the PPMS instrumentation. Research leading to these results received funding from the Research Council of Norway (FRINATEK project 221905).

References

[1] Amow G, Au J, Davidson I. Synthesis and characterization of $La_4Ni_{3-x}Co_xO_{10\pm\delta}$ ($0.0 \leq x \leq 3.0$, $\Delta x = 0.2$) for solid oxide fuel cell cathodes. Solid State Ionics. 2006;177;1837-1841

[2] Yoo S, Choi S, Shin J, Liu M, Kim G. Electrical properties, thermodynamic behavior, and defect analysis of $La_{n+1}Ni_nO_{3n+1+d}$ infiltrated into YSZ scaffolds as cathodes for intermediate-temperature SOFCs. RCS Advances. 2012;2;4648-4655

[3] Hansteen OH, Fjellvåg H. Synthesis, Crystal Structure, and Magnetic Properties of $La_4Co_3O_{10+\delta}$ ($0.00 \leq \delta \leq 0.30$). J Solid State Chem. 1998;141;212-220

[4] Zhang Z, Greenblatt M. Synthesis, Structure, and Properties of $Ln_4Ni_3O_{10-\delta}$ (Ln = La, Pr, and Nd), J Solid State Chem. 1995;117;236-246

[5] Goodenough JB, Raccah PM. Complex vs Band Formation in Perovskite oxides. J Appl Phys. 1965;36;1031-1032

[6] Fjellvåg H, Hansteen OH, Hauback BC, Fischer P. Structural deformation and non-stiochiometry of $La_4Co_3O_{10+\delta}$. J Mater Chem. 2000;10;749-754

[7] Olafsen A, Fjellvåg H, Hauback BC. Crystal Structure and Properties of $Nd_4Co_3O_{10+\delta}$ and $Nd_4Ni_3O_{10-\delta}$. J Solid State Chem. 2000;151;46-55

[8] Tkalich AK, Glazkov VP, Somenkov VA, Shil'shtein SS, Kar'kin AE, Mirmel'shtein AV, Synthesis, structure, and properties of nickelates $R_4Ni_3O_{10}$ (R = Nd, Pr, La). Superconductivity. 1991;4;2280-2286

[9] Carvalho MD, Cruz MM, Wattiaux A, Bassat JM, Costa FMA, Godinho M. Influence of oxygen stoichiometry on the electronic properties of $La_4Ni_3O_{10\pm\delta}$. J Applied Phys. 2000;88;544-549

[10] Pawley GS, Unit-Cell Refinement From Powder Diffraction Scans. J Appl Cryst. 1981;14;357-361

[11] Coelho AA. TOPAS. Version 4.2. BRUKER AXS: Germany; 2009

[12] Larson AC, Von Dreele RB. General Structure Analysis System (GSAS). Los Alamos National Laboratory: LAUR 86-748; 1994

[13] Heikes RR, Miller, RC, Mazelsky R. Magnetic and electrical anomalies in $LaCoO_3$. Physica. 1964;30;1600-1608

[14] Gilbu B, Fjellvåg H, Kjekshus A. Properties of $LaCo_{1-t}Cr_tO_3$. I. Solid solubility, Thermal Expansion and Structural Transition, Acta Chem Scand. 1994;48;37-45

[15] Gilbu Tilset B, Fjellvåg H, Kjekshus A, Hauback BC. Properties of $LaCo_{1-t}Cr_tO_3$. IV. Structure and Magnetism. 1998;52;733-744

[16] Durand AM, Belanger DP, Booth CH, Ye F, Chi S, Fernandez-Baca JA, Bhat M. Magnetism and phase transitions in $LaCoO_3$. J Phys Condens Matter. 2013;25;382203

[17] Yan J-Q, Zhou J-S, Goodenough JB. Ferromagnetism in $LaCoO_3$. Phys Rev B. 2004;70;014402

[18] Noguchi S, Kawamata S, Okuda K, Nojiri H, Motokawa M. Evidence for the excited triplet of Co^{3+} in $LaCoO_3$. Phys Rev B. 2002;66;094404

[19] Podlesnyak A, Streule S, Mesot J, Medarde M, Pomjakushina E, Conder K, Tanaka A, Haverkort MW, Khomskii DI. Spin-State Transition in $LaCoO_3$: Direct Neutron Spectroscopic Evidence of Excited Magnetic States. Phys Rev Lett. 2006;97;247208

[20] Hsu H, Blaha P, Wentzcovitch RM, Leighton C. Cobalt spin states and hyperfine interactions in $LaCoO_3$ investigated by LDA+U calculations. Phys Rev B. 2010;82;100406

[21] Yamaguchi S, Okimoto Y, Tokura Y. Local lattice distortion during the spin-state transition in $LaCoO_3$. Phys Rev B. 1997;55;R8666-R8669

[22] Phelan D, Louca D, Rosenkranz S, Lee S-H, Qiu Y, Chupas PJ, Osborn R, Zheng H, Mitchell JF, Copley JRD, Sarrao JL, Moritomo Y. Nanomagnetic Droplets and Implications to Orbital Ordering in $La_{1-x}Sr_xCoO_3$. Phys Rev Lett. 2006;96;027201

[23] Vankó G, Rueff J-P, Mattila A, Németh Z, Shukla A. Temperature- and pressure-induced spin-state transitions in $LaCoO_3$. Phys Rev B. 2006;73;024424-1-024424-9

[24] Cotton FA, Wilkinson G. Advanced inorganic chemistry. New York: Wiley; 1972

[25] Hansteen OH, Fjellvåg H, Hauback BC. Powder Neutron and X-Ray Diffracion Study of $La_4Co_3O_{10.00}$. Chem Papers. 1998;52;7-11

[26] Kobayashi Y, Taniguchi S, Kasai M, Sato M, Nishioka T, Kontani M. Transport and Magnetic Properties of $La_3Ni_2O_{7-\delta}$ and $La_4Ni_3O_{10-\delta}$. J Phys Soc Jpn. 1996;65;3978-3982

[27] Greenblatt M. Ruddlesden-Popper $Ln_{n+1}Ni_nO_{3n+1}$ nickelates: structure and properties. Curr Opin Solid State Mater Sci. 1997;2;174-183

[28] Shannon RD. Revised Effective Ionic Radii and systematic Studies of Interatomic Distances in Halides and Chalcogenides. Acta Cryst. 1976;A32;751-767